Nine tiny star clusters in Gaia DR1, PS1 and DES

G. Torrealba,[1][*] V. Belokurov,[2,3] S. E. Koposov[4,2]

[1] *Institute of Astronomy and Astrophysics, Academia Sinica, P.O. Box 23-141, Taipei 10617,Taiwan*

[2] *Institute of Astronomy, University of Cambridge, Madingley Road, Cambridge CB3 0HA, UK*

[3] *Center for Computational Astrophysics, Flatiron Institute, 162 5th Avenue, New York, NY 10010, USA*

[4] *McWilliams Center for Cosmology, Department of Physics, Carnegie Mellon University, 5000 Forbes Avenue, Pittsburgh, PA 15213, USA*

ABSTRACT

We present the results of a systematic Milky Way satellite search performed across an array of publicly available wide-area photometric surveys. Our aim is to complement previous searches by widening the parameter space covered. Specifically, we focus on objects smaller than $1'$ and include old, young, metal poor and metal rich stellar population masks. As a result we find 9 new likely genuine stellar systems in data from GAIA, DES, and Pan-STARRS, which were picked from the candidate list because of conspicuous counterparts in the cut-out images. The presented systems are all very compact ($r_h < 1'$) and faint ($M_V \gtrsim -3$), and are associated either with the Galactic disk, or the Magellanic Clouds. While most of the stellar systems look like Open Clusters, their exact classification is, as of today, unclear. With these discoveries, we extend the parameter space occupied by star clusters to sizes and luminosities previously unexplored and demonstrate that rather than two distinct classes of Globular and Open clusters, there appears to be a continuity of objects, unmarked by a clear decision boundary.

Key words: Galaxy: halo, galaxies: dwarf, Magellanic Clouds

1 INTRODUCTION

Is there a sea of undiscovered faint satellites out there in the halo of the Galaxy? Chances are, there is, given the avalanche of recent discoveries (see e.g. Koposov et al. 2015; Bechtol et al. 2015) and the theoretical expectations (Koposov et al. 2008; Tollerud et al. 2008; Koposov et al. 2009; Jethwa et al. 2018). With the data from ambitious all-sky surveys and smaller targeted campaigns, dwarf galaxies and star clusters are now identified routinely at levels of surface brightness previously unimaginable (for reviews, see Willman 2010; Belokurov 2013). The extension of the spectrum of Galactic fragments into such low luminosity regime is not only a compelling evidence for the hierarchical structure assembly, but also a convenient benchmark of the (currently poorly constrained) star-formation theory (see e.g. Koposov et al. 2009; Peñarrubia et al. 2012; Brooks & Zolotov 2014).

Star clusters (like those presented in this work) are the faintest (and the smallest) of the newly identified satellites (e.g. Belokurov et al. 2014; Laevens et al. 2014; Kim & Jerjen 2015; Kim et al. 2015; Koposov et al. 2017; Luque et al. 2017, 2018). Not only are these hard to find, they are also notoriously problematic to characterize, as their in-

ner regions suffer from heavy blending if observed from the ground. While, in principle, there should be a continuous distribution of cluster properties, it is customary to divide them into two groups: Globular and Open (GCs and OCs). GCs are denser, older and more luminous, OCs are more sparse, contain fewer stars and are substantially younger.

There also appears to be a dichotomy as to the habitat of each species. In general, OCs are located around the Galactic plane while GCs wander in the halo. Such difference in spatial distribution betrays the difference in the birth place. OCs have presumably been born in the Milky Way's disk while the majority of GCs must have been accreted and their former hosts destroyed (see e.g. Zinn 1993; Mackey & Gilmore 2004; Mackey et al. 2010). In particular, a subpopulation of the halo GCs with intermediate ages (also known as young halo clusters) appear to have properties indistinguishable from those clusters found in external galaxies (Mackey & Gilmore 2004). Even if a direct comparison is not possible, properties of the stellar populations give away the GCs' origin, as it is the case of a group of stray halo clusters which follow the same age-metallicity relationship as that of the stars in the Sgr dwarf galaxy (see e.g. Marín-Franch et al. 2009).

Importantly, the halo GCs possess the key information as to the accretion history of the Galaxy: their ages can be
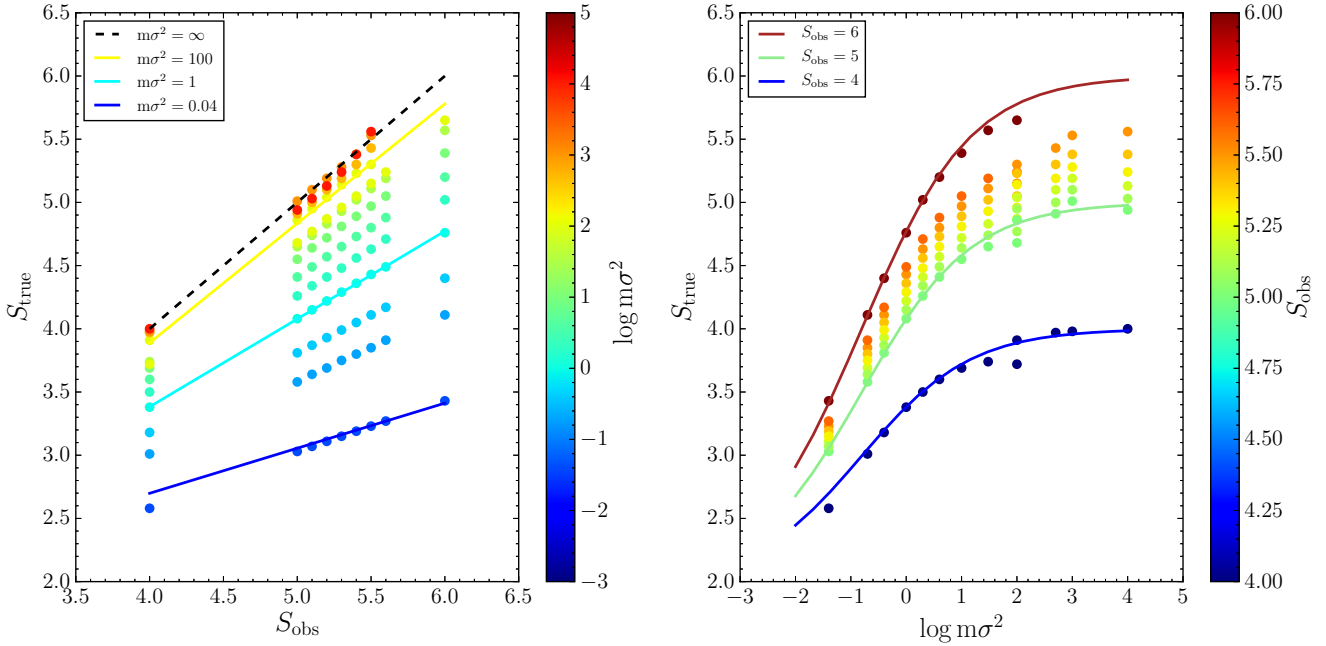
Figure 1. Comparison between the real significance and the measured significance is shown in the left panel for the Poisson noise simulations. The colored lines shows the empirical fit given by equation 2 with the logarithm of the stars per kernel shown in color. The black dashed line is the 1 to 1 line. Note the evident difference between the real and measured significances for low number of stars and how the correction is able to recover the real significance from the measured significance. In the right panel, we show the real significance as a function of stars per kernel for different measured significances. The lines shows the real significance calculated from the measured significance.

used to date the past merger events. This sort of evidence is vital for dynamical modelling of the halo assembly, but not directly available otherwise (see, however, de Boer et al. 2015). Intriguingly, detailed studies of many of the recently discovered faint halo star clusters confirm that these too are significantly younger than the quintessential old halo GCs. For example, Whiting 1 is estimated to be 5 Gyr old (Carraro 2005), Gaia 1 and 2, 6 and 8 Gyr correspondingly (Koposov et al. 2017), even Segue 3, originally deemed to be truly old (Fadely et al. 2011), is claimed to have an age of ~3 Gyr (Ortolani et al. 2013). With extremely low stellar densities and (allegedly) young ages, these newly discovered clusters appear to look more like OCs than GCs.

A deluge of star clusters is now entering the Milky Way, dragged in with their current host, the Large Magellanic Cloud (LMC). The LMC boasts an impressive array of star clusters: the early catalogue of Kontizas et al. (1990) lists 1762 candidates, while Bica et al. (2008) announces a record number of 3740 clusters, but even today new clusters are being added (see Sitek et al. 2017), which suggests that the star cluster census is still incomplete. Furthermore, only a fraction (687) have well- measured structural parameters (Werchan & Zaritsky 2011). The LMC's rich collection of star clusters has long been used to good effect to forward our understanding of emergence and development of structure on small scales. This is illustrated by studies of star cluster dynamical evolution in general (see e.g. Elson et al. 1987), and under tidal stresses in particular (Bica et al. 2015). Detailed analysis of the LMC's star-formation history was possible thanks to the availability of a large number of star

clusters with ages and metaillicities (see e.g. Girardi et al. 1995; Harris & Zaritsky 2004; Glatt et al. 2010; Palma et al. 2015). Additionaly, star clusters are perfect tracer particles to probe the structural properties of the Clouds themselves (see e.g. Bica et al. 2008, for the latest effort).

As samples of new faint objects continue to grow rapidly, selection biases become more apparent. Almost all satellites discovered in this century have been found as stellar over-densities in large photometric datasets. These searches typically start by creating density map of stars, and convolving them with different kernels to estimate the local density of stars and the local background density. Then, by comparing the two densities, one can compute a statistical significance, which is then used to create a list of candidates (see Irwin 1994). Evidently, at low levels of statistical significance, these algorithms begin to incur a sharply increased rate of false positives. To keep the satellite selection contaminant-free and to avoid as much of visual inspection of candidates as possible, it is customary to accept objects at the significance levels higher than dictated by the probability of a chance fluctuation. More worryingly, the estimate of the significance itself can be biased, for example in the case of a small number of stars per kernel or in the presence of galaxy contamination.

Within a wide range of distances, sizes and luminosities, both globular clusters and dwarf galaxies can reveal themselves as a compact excess of stars above the smoothly-varying Galactic density background. Indeed, if a satellite is resolved into stars, our satellite searching method can be employed to pinpoint its location in the sky. It would be prefer-
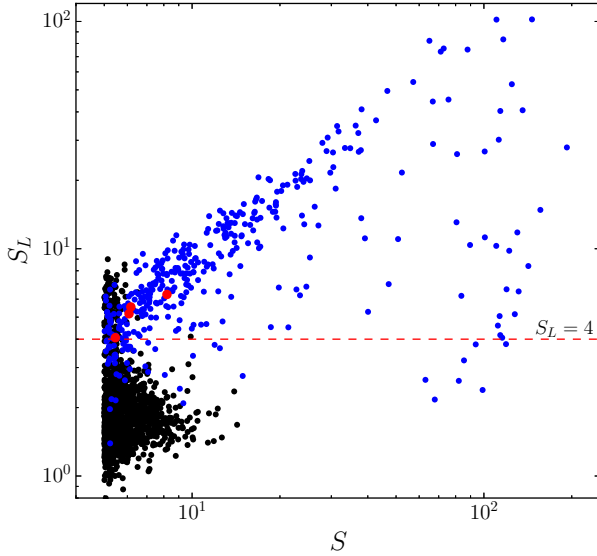
computationally more expensive and/or might be severely biased if small number statistics are not taken into account. In this work, and as a way to complement previous searches, we have run a search for small clusters in a set of publicly available surveys. The method used closely follows the one presented in Torrealba et al. (2018), in which we first filter the desired stellar population, create a density map of stars and convolve it with two kernels: an inner kernel to estimate the local density, and an outer kernel to estimate the background. We then estimate two significances, the "true" significance S, in which we compare the local density with the expected variance, and a local significance S_L, which helps to identify problematic areas in which the variance is underestimated. S_L is defined based on the properties of S around an overdensity:

$$S_L = \frac{S(0) - \langle S_{d<\sigma_o} \rangle}{\sqrt{\mathrm{Var}\left(S_{d<\sigma_o}\right)}}, \qquad (1)$$

where $S(0)$ is the significance at the center of an overdensity, σ_o is the width of the outer kernel, and $S_{d<\sigma_o}$ are the significances for all pixels within σ_o from the center. In areas where the variance is underestimated, S is overestimated and then $\langle S_{d<\sigma_o} \rangle \gg 0$, which means $S_L \ll S$. This allows us to cull false positives by simply selecting overdensities that have both large S and large S_L.

Specifically, we do a search with two very small inner kernels (0.3′ and 1′)[1] using a combination of young and old isochrones (log (age [yr]) = 10.1, 9.8 and 9.6, we will use these units when referring to age throughout the paper) with two different metallicities ([Fe/H] = −2 and −1), allowing us to probe a more extended parameter space than the one typically explored. We use distance moduli between 16 and 21, which lets us explore the halo for satellites between ∼ 16 kpc and ∼ 150 kpc, and use an outer kernel of 10′, whose small size is only possible due to the small inner kernel size. This allows the large kernel to be sensible to rapidly changing areas like the outskirts of the Magellanic Clouds or the galactic disk.

2.1 Correction for small number of counts

In the satellite search procedure described in Torrealba et al. (2018) it is implicitly assumed, that the result of the convolution of density maps is Gaussian distributed. However this approximation is bound to break if the number of stellar tracers within the inner kernel drops low enough. This can happen if a particularly rare type of stars is used, e.g. Blue Horizontal Branch stars (BHBs), or, simply when the kernel size is small enough, like in the case presented in this work. This non-Gaussianity of the distribution will affect the the tail probability caclulations and if ignored will lead to overestimated statistical significances that produce an increase in the number of false positive detections.

In what follows, we provide a simple correction for the significance estimation in the case of low number of counts.

Figure 2. Significance verus local significance for detections in Gaia with 1′ kernel. Candidates are shown in black, previously known MW stellar systems are shown in blue, and new discoveries are shown in red. The objects below the $S_L = 4$ line are excluded to produce a cleaner candidate list. This cut is largely supported from the locus that known objects occupy in the plot, which is shared by the new discoveries.

able if such a catalogue-based search depended as little as possible on the satellite's structural parameters and/or its stellar populations properties. Therefore, in our approach, we first cast the net as wide as possible to pick out as many statistically significant stellar over-densities as possible. The result of the first step of our algorithm is a list of over-density candidates ranked by their significance. As a second step, we construct a set of test statistics to further assess the reality of the pre-selected candidates. The most relevant of these involves the modeling of each individual candidate to determine whether the distribution of their stars in the sky and magnitude space, resembles that of a genuine satellite (i.e. an agglomeration of stars evolving together at the same Galacto-centric distance).

In this work we choose to conduct a satellite search using a version of the well-established satellite search algorithm (see Torrealba et al. 2016a, 2018) to look for small/compact objects ($r < 1′$) in the publicly available data from different surveys. Several groups (including ourselves) have already combed these data for the most obvious new objects. However, the question of robust detection of systems at the low significance end has not been addressed in detail. Additionally, no extensive search for small size satellites has been carried out. As a result of the search, we found 9 new stellar systems across the sky.

2 ALL SURVEYS SEARCH

Most wide-area optical surveys have already been mined for satellites, but typically aiming at old metal poor populations (e.g. Koposov et al. 2015). Moreover, searches for objects with sizes smaller than 1′ are often avoided as they are

---

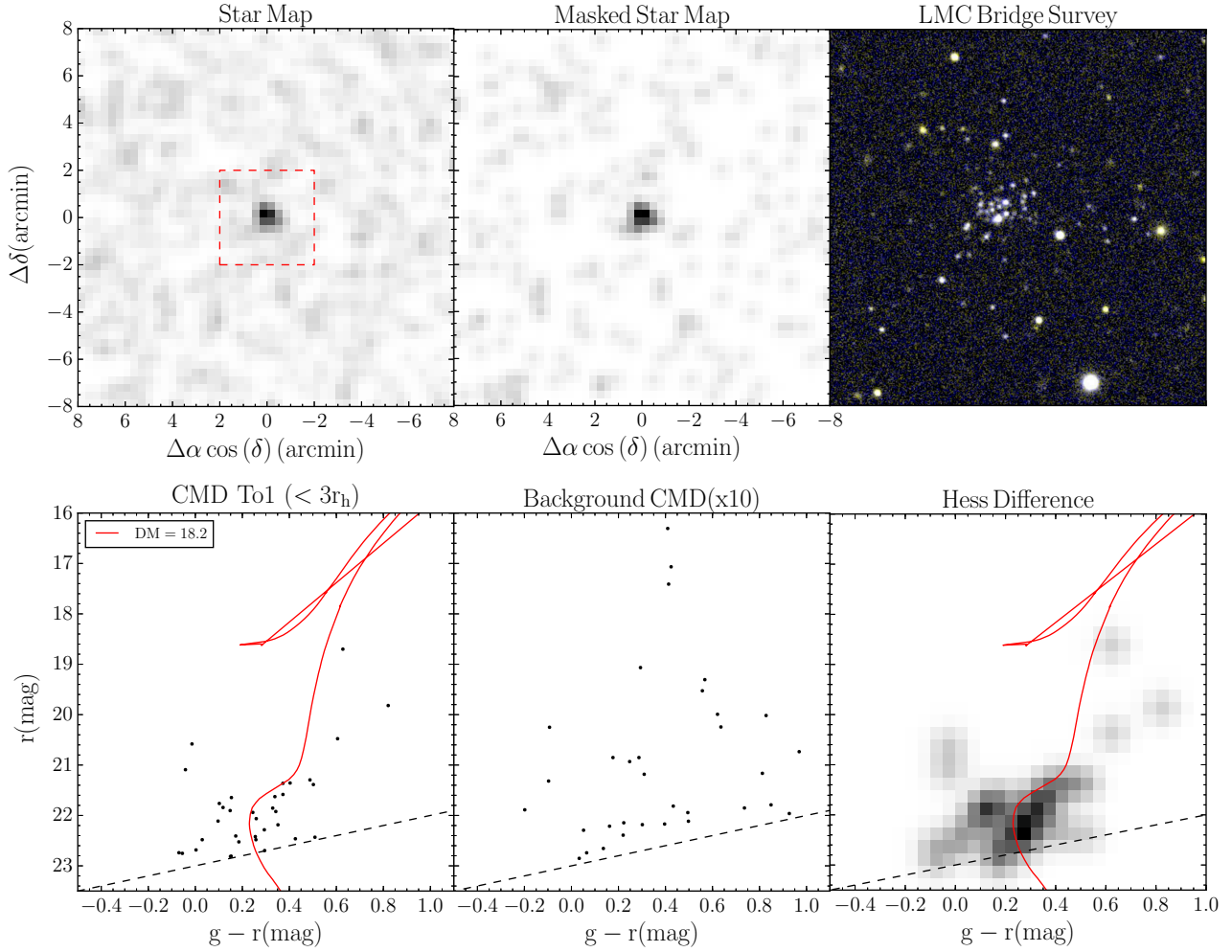[1] The smaller kernel size was picked based on available resources at the time.

Figure 3. Discovery plot of To 1 in MC bridge survey data. In the top row, left panel shows a density map of the stars in the region, middle panel shows a density map of stars within the isochrone mask of the best fit isochrone, and the rightmost panel shows a false color image of the region marked with the red dashed square in right panel. In the bottom row, left panel shows the CMD of the stars within 3 half light radius of the best fit model, and the best fit isochrone in red. The dashed black line shows the approximate magnitude limit of the survey in this region. The middle lower panel shows the CMD of the background/foreground stellar population for ten times the area used in the lower left panel, the right lower panel shows the Hess difference diagram. The CMD shows a very clear turn off and a sparsely populated red giant branch, in a region where the expected background is scarce. Indeed, it is so sparse that in order to see it, we used an area 10 times bigger than the area used for the satellite. The compactness and luminosity of To 1 are consistent with a faint globular cluster at ∼ 43.6 kpc. Located about ∼ 12 kpc from the LMC, it is highly likely part of its globular cluster system.

This is achieved by computing the statistical significance values (Z-values) for an array of simulated datasets and comparing those to the true probabilites of a random fluctuation to find an empirical relation between them. Our mock data are 2D pixel grids with each pixel value following the Poisson distribution. These are then convolved with kernels of different sizes, and the observed significance, $S_{\rm obs}$, is computed. Next, by counting the number of pixels above a given value of $S_{\rm obs}$ and comparing it to the total number of pixels, we can measure the real probability - which we can in turn transform to real significance $S_{\rm true}$ - of observing a value larger than $S_{\rm obs}$ due to random fluctuations. Figure 1 shows the behavior of the true significance $S_{\rm true}$ as a function of the measured one. As illustrated by the Figure, the bias induced

by the assumption of Gaussianity is a strong function of the number of stars within the kernel $N_{\rm sk} = m\sigma_s^2$, where m is the average number of stars per pixel and σ_s is the width of the inner kernel. For example, for 10 stars per kernel, while the observed significance is reasonably high $S_{\rm obs} \sim 5$, the true significance is much lower with $S_{\rm true} \sim 4$. The bias is exacerbated when the number of stars per kernel plummets as low as ∼1: the true significance drops to ∼3.

To correct for this effect, we find that the dependence

of S_{true} as a function of S_{obs} and N_{sk} can be empirically fitted by the following model:

$$S_{\text{true}} = \frac{S_{\text{obs}} + 2aN_{\text{sk}}^{-a}}{1 + aN_{\text{sk}}^{-a}}, \tag{2}$$

where $a = 1/\ln 10 \approx 0.434$.

As Figure 1 illustrates, the above formula provides a satisfactory approximation of the evolution of the true significance across a wide range of the observed significance values as well as the kernel sampling values. We apply this correction to S only, before estimating S_L.

2.2 Satellite Modeling

An additional step of our search algorithm consists of a detailed study of the probability of our candidates to be a real satellite. At this point, the candidate's structural parameters are derived, and when color information is available, distances, ages, metallicities and luminosities are also derived. Models are fit simultaneously to the distributions of the candidate's stars (and the associated background) in both the celestial coordinates and the CMD (see e.g. Martin et al. 2008; Koposov et al. 2010, for a similar approach).

The probability of observing a star at a position in 4D space, $\mathbf{\Phi}$, spanned by 2 spatial coordinates, a color, and a magnitude, $\mathbf{\Phi} = (\mathbf{\Phi_s}, \mathbf{\Phi_c}) = ((x, y), (\text{col}, \text{mag}))$ is:

$$\begin{aligned} P(\mathbf{\Phi}|\gamma) =& f P_s^{obj}(\mathbf{\Phi_s}|\gamma_s) P_c^{obj}(\mathbf{\Phi_c}|\gamma_c) + \\ & (1-f) P_s^{bg}(\mathbf{\Phi_s}|\gamma_s) P_c^{bg}(\mathbf{\Phi_c}|\gamma_c), \end{aligned} \tag{3}$$

where f is the fraction of stars that belong to the object, the suffixes s and c refer to the coordinates on the sky and the CMD, respectively. γ is a shorthand for the model parameters, bg refers to the background model, and obj refers to the satellite model.

2.2.1 Celestial distribution model

To avoid distortions in the shape of the models, the spatial fitting of the candidates is performed in a gnomonic projection of the equatorial coordinates. In the projected space $\mathbf{\Phi_s} = (x, y)$, the object is modeled as a 2D elliptical plummer sphere:

$$P_s^{obj}(\mathbf{\Phi_s}|\gamma_s) = \frac{1}{\pi a^2 (1-e)} \left(1 + \frac{\tilde{r}^2}{a^2}\right)^{-2}, \tag{4}$$

where $\tilde{r}^2 = \tilde{x}^2 + \tilde{y}^2$ and

$$\begin{bmatrix} \tilde{x} \\ \tilde{y} \end{bmatrix} = \begin{bmatrix} \cos\theta/(1-e) & \sin\theta/(1-e) \\ -\sin\theta & \cos\theta \end{bmatrix} \begin{bmatrix} x - x_0 \\ y - y_0 \end{bmatrix}. \tag{5}$$

Then, the spatial model has 5 parameters: the center of the plummer profile (x_0, y_0), the half light radius a, the ellipticity e, and the orientation of the ellipse θ.

We model the background stellar distribution with a bilinear distribution of the form:

$$P_s^{bg} = \frac{1}{N_s^{bg}}(p_1 x + p_2 y + 1), \tag{6}$$

where p_1 and p_2 define the strength of the gradient in the east-west and north-south directions respectively, and N_b is defined so P_s^{bg} is normalized over the modeled area. In total, the spatial model has 7 free parameters, 5 for the objects and two for the background.

2.2.2 Color Magnitude distribution model

When color information is available (i.e. when at least two magnitudes are available), we model the distribution of the stars in the CMD space by binning it into a 2D histogram and quantifying the probability of finding a star, from background or satellite, in each bin. For the satellite, the PDF is defined based on the mass function of the PARSEC isochrones (Bressan et al. 2012). Specifically, the probabilities of finding a star in each bin are found in three steps: First, we select an isochrone with a given metallicty and age, and shift it to an specific distance. Second, we find the number of stars along the isochrone track - as given by the isochrone mass function - and populate the binned CMD. Finally, we convolve the populated CMD with the corresponding photometric errors - directly drawn from the data - and normalize the binned CMD so the integral over it is 1. By this definition, the CMD model of the satellite has only three free parameters, namely, the isochrone age, the isochrone metallicity, and the distance modulus.

For the background model of the CMD space, the process is much simpler. We create it empirically from the stars around the candidate, and bin them in a 2D CMD histogram with the same shape as the one defined for the satellite model. Then, after convolving the histogram with a small Gaussian kernel to make it smoother, we normalize it so the integral sums to 1.

Summarizing, the full model takes 2D positions on the sky and two magnitudes as input, and has a total of 11 free parameters. These include the isochrone parameters - age, metallicty, and distance - that define the CMD model. The spatial model is determined by the center, size, ellipticity, and position angle of the plummer model, plus two extra parameters to define the background. And finally, the fraction of stars that belong to the satellite. To fit the model to each candidate, we select the stars within one outer kernel from its center, and find the maximum likelihood solution, first for a background only model (i.e. $f = 0$), and second for the full model described above. This allows us to compute the log-likelihood difference, ΔL (of the model that contains the satellite versus the model composed of background only), giving a new significance criterion to assess if the overdensity correspond to a real stellar system or not.

2.3 Nine new satellites

We applied the algorithm with the mentioned setup to the first data release of GAIA (Gaia Collaboration et al. 2016), the first data release of PanSTARRS (Chambers et al. 2016), the LMC/SMC bridge survey by Mackey et al. (2018), the DES year 1 catalogue produced by Koposov et al. (2015), ATLAS (Shanks et al. 2015), and the SDSS data release 9 (Ahn et al. 2012). For every survey, we then create a list of candidates that have $S_L > 4$, to ensure they are isolated compact objects, and sort them by significance. The impact

of such selection criteria can be seen in Figure 2, which shows S versus S_L for all objects detected in Gaia with $1'$ kernel. Previously known genuine stellar systems are shown in blue, unknown detections in black. The systems presented in this work (see below) are shown in red. The importance of S_L for small S is evident. A simple cut in S_L can remove most of the - alleged - false positives without removing many good detections, allowing for a clean and manageable list of candidates. To avoid the need of follow up, and given that one expects to see a counterpart in the image for the compact objects sought from this search, we only picked candidates that were almost unequivocally confirmed by visual inspection. Then, by going through the lists of candidates - and visually inspecting the first hundred candidates in each survey - we were able to identify 8 unknown highly likely real stellar systems. To this list we also add a serendipitously discovered globular cluster that lies in a chip gap in the original DES catalogue generated by Koposov et al. (2015).

Of the 9 objects selected, 5 correspond to discoveries made with Gaia. As pointed out by Koposov et al. (2017), Gaia possess unique capabilities that make it very well suited to search for stellar systems resolved into stars. In particular, its high resolution allows for an efficient star/galaxy separation and star detection in crowded areas. Also, the multi-epoch observation strategy allows for the removal of spurious detections, like the ones produced by bright stars. The last point proved to be particularly relevant since the brightest star in the sky was responsible for hiding a very prominent star cluster (i.e. Gaia 1 Koposov et al. 2017) - in a frequently visited area of the sky - until now. One of the clusters presented here, Gaia 7, is also obscured by a bright star.

2.4   Multi-band photometry analysis

The availabilty of multi-band photometry allows for the inference of physical and stellar population properties of the stellar systems. Here we present the result of the modelling of the nine star cluster candidates using the isochrone fitting technique. This fit allows us to estimate satellite's distances and luminosities. For the five systems initially found in Gaia data, we used deeper available data. Specifically, three of the Gaia satellites had Pan-STARRS data, the other two fell into the footprints of SMASH, in the case of Gaia 3, and DeCAPS, in the case of Gaia 6. Of the remaining satellites, 2 were discovered in DES, one was discovered in the MC bridge survey (Mackey et al. 2018), and the last one was detected in the Pan-STARRS data. The detailed summary together with the main physical properties inferred can be found in Table 1.

To 1 is the most prominent of the discoveries presented in this paper. It is identified in the MC bridge survey and boasts an unambiguous detection significance of 16.5. The discovery plot for To 1 is given in Figure 3. Top panels display the spatial information, and the bottom panels show the CMD information. To 1's signal is obvious across all panels, with a CMD harboring a strong main sequence turn-off (MSTO) together with a small number of plausible RGB candidates. The best-fit isochrone, shown in red, is consistent with an old and metal poor population at ~ 43.5 kpc, placing To 1 only ~ 7 kpc away from the LMC. It has an absolute magnitude of $M_V \sim -1.6$ and a physical size of ~ 3.5

pc, thus placing it in a region of the size-luminosity plane below the main locus of globular clusters. This region have been gradually populated with various discoveries in the last 10 years (e.g. Koposov et al. 2007; Balbinot et al. 2013; Kim et al. 2016). Its position in the sky, as well as its physical properties, suggest that To 1 may be associated with the MCs.

Gaia 3's discovery is shown in Figure B1. Originally found in Gaia with a significance in excess of 8, Gaia 3 is the second most prominent detection presented in this work. Coincidentally, Gaia 3 happens to lie in one of the pointings of the SMASH survey (Nidever et al. 2017), but the associated data is not available as part of their first data release. Nevertheless, the stacked images are publicly available through the NOAO Science Archive (NSA). Although data for this part of the sky is already provided in the NOAO source catalogue (NSC, Nidever et al. 2018), most sources in the central parts of Gaia 3 were missing, probably due to crowdedness. Consequently, we re-analyzed the SMASH g-band and r-band stacked images with a simple SExtractor+PSFex combo (Bertin & Arnouts 1996), allowing for higher de-blending, and calibrated it using the NSC. With the resulting catalogue, we can easily see Gaia 3 in the density maps and in the CMD. Indeed, Gaia 3 is well fit by our stellar+spatial model (with a likelihood difference of $\Delta L \sim 90$). The best fit reveals that Gaia 3 is a compact $r_h \sim 0.4'$ relatively luminous stellar system ($M_V \sim -3.3$) located at $D_H \sim 49$ kpc with $\log(age) \sim 9.1$ and a metallicity of [Fe/H] ~ -1.8. Located ~ 6 degrees away from the LMC, its position and characteristics reflects those of the LMC cluster system, suggesting a Magellanic origin. This cluster is perhaps a prime example of how the combination of Gaia, with its superb astrometry, plus the small spatial scales used in this work can reveal previously undiscovered - but very prominent - stellar associations.

Gaia 4 is shown in Figure B3. Like Gaia 7, it is located very close to the Galactic disk ($b \sim -1.5$) in a region of high extinction and within the Pan-STARRS footprint. The overdensity of stars can be easily seen in the Pan-STARRS density maps, and the photometry reveals a well-defined MS. As a result we are able to get a good fit of its structural and stellar population properties. Gaia 4 is found to be composed of a compact ($r_h \sim 1.17'$) stellar population at $DM \sim 13.7$ with $\log(age) \sim 9$ and a metallicity of [Fe/H] $= -0.1$, and it is the second most luminous object presented in this work with $M_V \sim -2.4$. But even at this luminosity, and a relatively high significance ($S \sim 7.5$) in our Gaia searches, it was still missing in previous Pan-STARRS searches. Perhaps this is due to a combination of the satellite's small size and a high (and variable) extinction in the region. Given its position in the disk, low luminosity, small size, and the lack of a well defined center in the false-color image, it looks like Gaia 4 is probably another Galactic open cluster.

PS1 1/Prestgard 64 is the only detection procured when applying the search algorithm to the Pan-STARRS data.PS1 1 was also independently identified by amateur astronomer Trygve Prestgard in DSS data in 2016 as Prestgard 64[1]. In PS1 data, it can be confidently reported as a genuine stellar system without the need of a follow-up as shown in Figure B4. At the center of PS1 1 an evident stellar overdensity is visible both in the cutout images as well as the density maps. The main feature of PS1 1 in the CMD
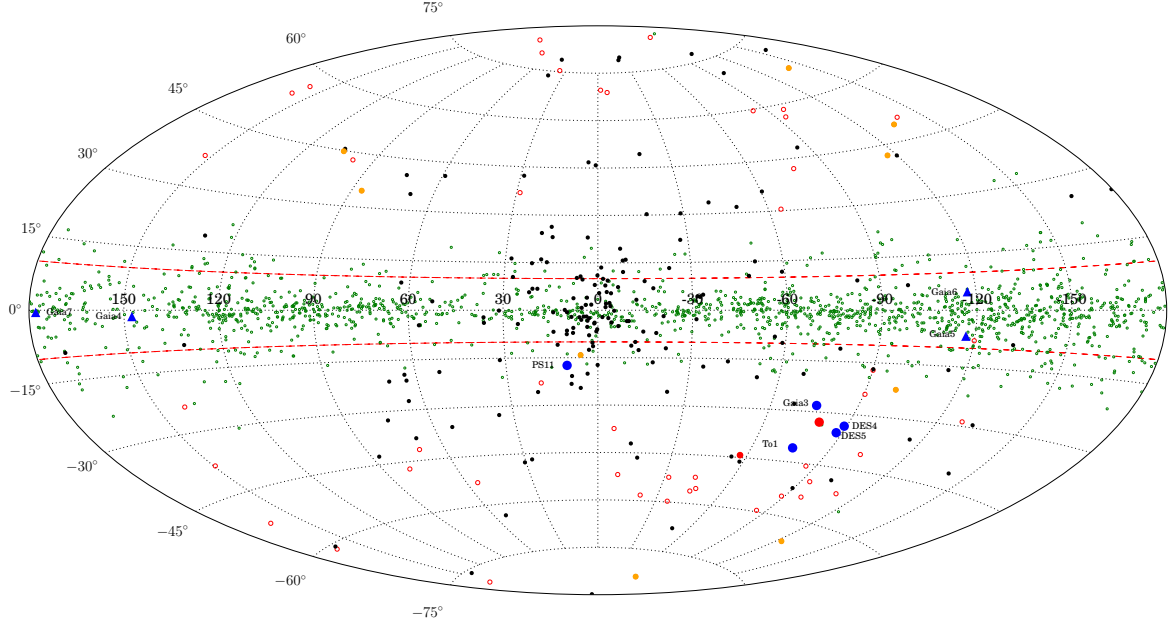
Figure 4. Spatial distribution of GCs and dwarf galaxies around the MW in galactocentric coordinates. Yellow markers shows the position of the Classical dwarfs, open red circles shows the position of other MW galaxies (from McConnachie (2012) plus Crater 2 (Torrealba et al. 2016a), Aquarius 2 (Torrealba et al. 2016b), DESJ0225+0304 (Luque et al. 2017), Pictor II (Drlica-Wagner et al. 2016), Virgo I (Homma et al. 2016), Cetus III (Homma et al. 2018), and Car II and Car III (Torrealba et al. 2018)), black dots the position of MW GCs (Harris 2010; Belokurov et al. 2010; Muñoz et al. 2012; Balbinot et al. 2013; Kim & Jerjen 2015; Kim et al. 2015, 2016; Laevens et al. 2015; Weisz et al. 2016; Luque et al. 2016, 2017; Martin et al. 2016; Koposov et al. 2017), and green open dots show the position of MW OCs (from Kharchenko et al. 2013). The new discoveries are shown in blue. The red dashed lines shows $|b| = 10 \deg$. 4 of the new discoveries, namely, Gaia 3, DES 4 and 5, and To 1 are very close to the LMC, and likely members of its GC population. The remaining 4 systems, Gaia 4 to Gaia 7, are located well within the disk, and are likely open clusters.

Table 1. Properties of clusters with isochrone fit

Name	RA (deg)	Dec (deg)	S	ΔL	r_h (′)	DM (mag)	D_h (kpc)	M_V (mag)	r_h (pc)	N_{star} [a]
To 1	56.08255	-69.42255	16.5	88.9	0.27	18.2	43.6	-1.6	3.45	33
Gaia 3	95.05864	-73.41445	8.2	89.8	0.53	18.4	48.4	-3.3	7.45	86
Gaia 4	56.36793	52.89297	7.5	46.1	1.17	13.7	5.4	-2.4	1.85	58
PS1 1	289.17121	-27.82721	6.3	49.6	0.55	17.4	29.6	-1.9	4.69	42
Gaia 5	110.79779	-29.71947	6.2	26.7	1.01	14.2	6.8	-0.1	2.01	20
Gaia 6	122.09798	-23.70648	6.1	55.4	1.20	11.9	2.4	0.2	0.85	101
Gaia 7	84.69075	30.49822	5.5	15.5	0.70	13.0	4.0	-1.8	0.82	13
DES 4	82.09501	-61.72369	5.1	13.0	0.83	17.5	31.3	-1.1	7.58	42
DES 5	77.50351	-62.58046	-	13.4	0.18	17.0	24.8	0.3	1.31	10

[a] N_{star} is the measured number of the system member stars above the limiting magnitude

Table 2. test

diagram is a clump of stars at $r \sim 21$. The maximum likelihood fitting favors a model in which this feature is explained by the MSTO of a stellar population at $DM = 17.4$, which yields a luminosity of $M_V \sim -1.9$ and a half light radius of $r_h \sim 4.7$ pc, which is consistent with both a GC or an OC classification.

Gaia 5 and 6 discovery plots are shown in Figure B7 and B8. The two satellites fall within the Pan-STARRS footprint, but were missed by previous searches - and our own Pan-STARRS search - likely because of their proximity to the Galactic disk ($|b| \lesssim 5 \deg$). Gaia 6 is also within the DEcam Plane Survey footprint (DECaPS Schlafly et al. 2018), and we use their first public data release to measure the physical and stellar population properties of Gaia 6. Both Gaia 5 and 6 share very similar properties: they are located close to the sun ($D_h \sim 5$ kpc), are well embedded into the

Galactic disk, and have sizes of the order of 1 pc, and absolute magnitudes hovering just above $M_V \sim 0$. Based on their location, structural properties, and the appearance of the image cutouts, we can confidently classify them as Galactic open clusters. We note that a classical Cepheid is sitting close to the center of Gaia 5. The star has a period of 3.33 days and a an average magnitude of $V \sim 12.95$ (Otero 2006). Using the period-luminosity relation for classical Cepheids (Feast & Catchpole 1997), we find $DM \sim 15.85$ for the star. This is ~ 1.7 magnitudes off from the the DM found for the best fit isochrone, hence, we conclude that the Cepheid and the open cluster are likely unrelated.

Gaia 7 discovery is summarized in Figure B2. Similar to Gaia 1 (Koposov et al. 2017), the very first MW satellite discovered using the Gaia data, Gaia 7 is located next to a bright star. Regions next to very bright objects are severely affected by artifacts - due to saturation and diffraction - in other photometric surveys, but thanks to Gaia, which excels at the removal of such spurious detections (see e.g. Fabricius et al. 2016), these regions are now accessible. Gaia 7 is located within the Pan-STARRS footprint, but while it is visible in its density maps, it was missed due to the proximity to the very bright star. Nevertheless, it is still clearly visible in the Pan-STARRS data. Indeed, as shown in Figure B2, Gaia 7 is easily visible both in Pan-STARRS images and density maps. Gaia 7 also features a well defined main sequence, to which we fit an isochrone while simultaneously model its on-sky distribution. As a result, we find that Gaia 7 is consistent with a relatively young population (log age~ 7.85) with [Fe/H] = 0.1 at $DM \sim 13.1$. We measure its half light radius to be $r_h \sim 0.42$pc and its absolute magnitude $M_V \sim 2.8$. These properties and its location let us confidently classify it as a Galactic open cluster. However, please note that the proximity of the bright star, as well as the high extinction in the region - E(B-V)~ 1.2, which means almost 4 magnitudes of extinction in g - could induce strong systematics in either the estimation of physical as well as stellar population properties.

DES 4 and DES 5, the two satellites discovered in the DES data, are both only a few degrees away from the LMC. Their discovery plots are shown in Figure B5 and Figure B6 respectively. Their CMDs are dominated by the LMC stars, which makes the isochrone mask of the target population very similar to the background. For this reason, DES 4 significance is quite low, and DES 5 was not even found in the search. However, both overdensities are extremely compact, and feature a conspicuous stellar overdensity in the false color images. In fact, DES 5 was serendipitously found while looking at images around the LMC to study the performance of the search in this region. Bear in mind that DES 5 was located in a chip gap in the original Koposov et al. (2015) catalogue, and hence missed from the searches, but with the first data release from DES (DR1, Abbott et al. 2018), the object is now completely sampled. In both cases the Hess difference diagram reveals an excess of stars that appears to be a part of a stellar population younger compared to the bulk of the LMC population. These CMD features are captured by the satellite model which we found to be more likely than the background-only model by $\Delta L \sim 13$. DES 4 has $M_V \sim -1.1$ and $r_h \sim 7.58$ pc, placing it at the interface between GCs, OCs, and Ultra-Faint Dwarfs (UFDs) in the size luminosity diagram. DES 5 fit is more compact

($r_h \sim 1.31$ pc) and much fainter ($M_V \sim 0.3$). Note that in both cases the high concentrations of stars in the object is likely affecting the photometry. This effectively means that some of the member stars missing from the catalogues. As a result, it is possible that both objects have their absolute luminosities underestimated by few 10^{-1} mags. For example, if DES 4 had 30% more stars, its luminosity will go up from $M_V = -1.1$ to $M_V = -1.4$.

3 CONCLUSIONS

We have presented a systematic search for compact stellar systems across different photometric surveys. Building on previous efforts (specially Koposov et al. 2008), we have added features to improve the detection of stellar systems, particularly at the faint end. Specifically, we provide a recipe to deal with the small number statistics, which allows for a search of very small objects without flooding the candidates list with false positives.

We have performed a search for satellite systems with sizes smaller than $1'$ in most available wide surveys, including Gaia, Pan-STARRS and DES. Even though these datasets have been mined for satellites before, we were able to detect 9 new stellar systems, highlighting the importance of the improvements in the detection procedure and the extension of the probed parameter space. Figure 4 shows the distribution of the new discoveries on the sky. New satellites are marked in blue. About half of the new satellites are close to the LMC, and are likely part of its star cluster system. The other half are located in the Galactic disk, where the bulk of the population of open clusters is sitting, hence likely OCs.

As Figure 5 demonstrates, the newly discovered satellites can all be found in the sparsely populated region in the left corner of the size-luminosity space. The new objects located in the Galactic disk, likely open clusters, are shown with triangles. Open clusters luminosities and sizes, estimated from the Kharchenko et al. (2013) open cluster catalogue, are shown in green, and forms a diagonal cloud in the diagram. This distribution closely resembles the two most characteristics limits in catalogue based searches of stellar systems, namely the limiting in magnitude and the limiting in surface brightness. This suggests that the current list of OCs is displaying strong selection effects. In this diagram, OCs are sitting just below GCs, but while they are both fainter and smaller, it appears that there is a smooth transition between the two groups, instead of a clear distinction. The new discoveries discussed in this paper are the faintest population in this diagram, sitting just below the OC loci, suggesting that they are perhaps just an extension of the OC population. Interestingly, both the OC catalogue and our searches are extremely incomplete in this region, especially in distance: none of the objects presented in this work are further than 50 kpc, and the OC catalogue is only complete out to ~ 2 kpc. It is then possible, if not expected, that a large population of faint but extended OCs is waiting to be found. Older OCs appear to be fainter and larger in the Kharchenko et al. (2013) catalogue, both traits that make them more difficult to find. This is in line with the apparent shortage of old OCs in the MW (Schmeja et al. 2014). However, given the results of our search, the objects
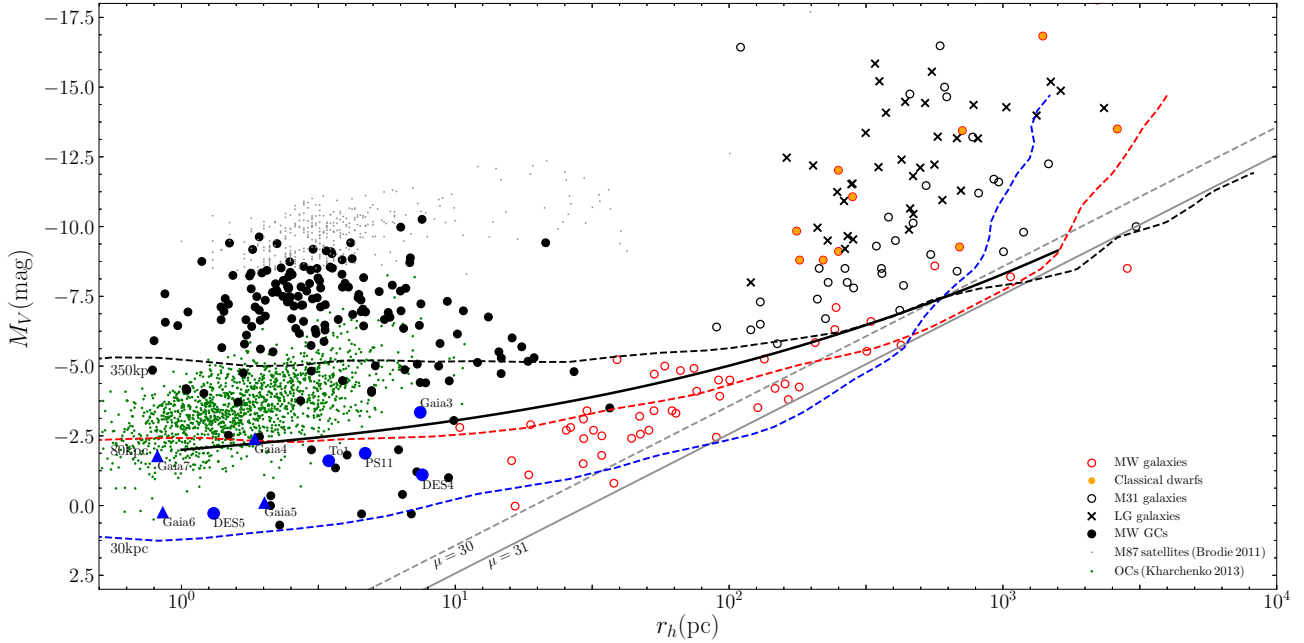
Figure 5. Absolute versus half light radius diagram. The markers are the same as Figure 4, plus M31 galaxies shown with black open circles, LG galaxies shown as black crosses (both from McConnachie 2012), M87 satellites shown in gray dots (from Brodie et al. 2011), and OCs are shown as open green dots (from Kharchenko et al. 2013). Lines of constant surface brightness at $\mu = 31$ and 30 are shown in gray continuous and dashed lines respectively. These roughly represent the detection limits of current surveys (Koposov et al. 2008, 2015). Lines of effective detection limits of the algorithm presented in this paper are shown as dashed blue, red, and black lines, representing the limits for satellites located at distances of 30, 80, and 350 kpc, respectively. The black line shows an effective limit of known satellites detected in Gaia DR1, above the line most satellites are detected, and below, most are missed. The new discoveries are shown in blue, with the objects sitting in the Galactic disk marked as triangles. Interestingly, they are mostly located in a sparsely populated region of the diagram, where classification is uncertain. The new discoveries are part of the population of the smallest and lowest luminosity stellar systems in the MW halo.

similar to those displayed here are common in the MW, thus starting to account for the alleged shortage.

Undoubtedly, one of the clear protagonists of this satellite search is Gaia. By covering the whole sky, Gaia allows for a holistic view of our Galaxy, including the bulge, the disks and the halo. Surprisingly, not only one can detect compact objects in Gaia, but it is also possible to detect some of the more luminous UFDs. This is illustrated with the black line in Figure 5, which gives the effective detection boundary for known MW satellites in Gaia: above the line we can detect known satellites across a wide range of sizes, but below the line most will be missed. While our current search in Gaia still suffers from a lot of drawbacks, namely, e.g. an unknown amount of spurious detections in the Gaia data (see e.g. the all sky view from Gaia DR1), it is clear that Gaia's is a wonderful dataset to study the halo, and particularly useful to build a homogeneous census of stellar systems across all latitudes. It is important to note that this search was carried out with the first data release of Gaia. The second data release provides significant improvements to the satellite detection capabilities. Particularly, the five-parameter astrometric solutions for 1.3 billion sources down to $G \sim 21$, as well as the photometry in blue and red passbands for a similar number of stars are ideal to survey the whole sky for nearby stellar systems. This can also be augmented by the information on 500 thousand variable stars,

which is a huge step forward compared to the Gaia DR1. As we have shown in this work, there is still much to be found in MW disk and halo, therefore all-sky, homogeneous surveys like Gaia can make an appreciable impact in the quest of characterizing MW structure and dynamics. Finally, while we have been able to update the census of stellar systems inside and in the outskirts of the MW and show that there is still room for unknown - relatively close - systems, our search is not completely automated. Indeed, in this instance we are still cherry-picking by selecting only the objects that can be identified in the image cutouts. There is plenty of room to improve the satellite search.

ACKNOWLEDGEMENTS

REFERENCES

Abbott T. M. C., et al., 2018, The Astrophysical Journal Supplement Series, 239, 18
Ahn C. P., et al., 2012, ApJS, 203, 21
Balbinot E., et al., 2013, ApJ, 767, 101
Bechtol K., et al., 2015, ApJ, 807, 50
Belokurov V., 2013, NARev, 57, 100
Belokurov V., et al., 2010, ApJ, 712, L103
Belokurov V., Irwin M. J., Koposov S. E., Evans N. W., Gonzalez-Solares E., Metcalfe N., Shanks T., 2014, MNRAS, 441, 2124
Belokurov V., Erkal D., Deason A. J., Koposov S. E., De Angeli F., Evans D. W., Fraternali F., Mackey D., 2017, MNRAS, 466, 4711
Bertin E., Arnouts S., 1996, A&AS, 117, 393
Bica E., Bonatto C., Dutra C. M., Santos J. F. C., 2008, MNRAS, 389, 678
Bica E., Santiago B., Bonatto C., Garcia-Dias R., Kerber L., Dias B., Barbuy B., Balbinot E., 2015, MNRAS, 453, 3190
Bressan A., Marigo P., Girardi L., Salasnich B., Dal Cero C., Rubele S., Nanni A., 2012, MNRAS, 427, 127
Brodie J. P., Romanowsky A. J., Strader J., Forbes D. A., 2011, AJ, 142, 199
Brooks A. M., Zolotov A., 2014, ApJ, 786, 87
Carraro G., 2005, ApJ, 621, L61
Chambers K. C., et al., 2016, preprint, (arXiv:1612.05560)
Drlica-Wagner A., et al., 2016, ApJ, 833, L5
Elson R. A. W., Fall S. M., Freeman K. C., 1987, ApJ, 323, 54
Fabricius C., et al., 2016, A&A, 595, A3
Fadely R., Willman B., Geha M., Walsh S., Muñoz R. R., Jerjen H., Vargas L. C., Da Costa G. S., 2011, AJ, 142, 88
Feast M. W., Catchpole R. M., 1997, MNRAS, 286, L1
Gaia Collaboration et al., 2016, A&A, 595, A2
Girardi L., Chiosi C., Bertelli G., Bressan A., 1995, A&A, 298, 87
Glatt K., Grebel E. K., Koch A., 2010, A&A, 517, A50
Harris W. E., 2010, preprint, (arXiv:1012.3224)
Harris J., Zaritsky D., 2004, AJ, 127, 1531
Homma D., et al., 2016, ApJ, 832, 21
Homma D., et al., 2018, Publications of the Astronomical Society of Japan, 70, S18
Irwin M. J., 1994, in Meylan G., Prugniel P., eds, European Southern Observatory Conference and Workshop Proceedings Vol. 49, European Southern Observatory Conference and Workshop Proceedings. p. 27
Jethwa P., Erkal D., Belokurov V., 2018, MNRAS, 473, 2060
Kharchenko N. V., Piskunov A. E., Schilbach E., Röser S., Scholz R.-D., 2013, A&A, 558, A53
Kim D., Jerjen H., 2015, ApJ, 799, 73
Kim D., Jerjen H., Milone A. P., Mackey D., Da Costa G. S., 2015, ApJ, 803, 63
Kim D., Jerjen H., Mackey D., Da Costa G. S., Milone A. P., 2016, ApJ, 820, 119
Kontizas M., Morgan D. H., Hatzidimitriou D., Kontizas E., 1990, A&AS, 84, 527
Koposov S., et al., 2007, ApJ, 669, 337
Koposov S., et al., 2008, ApJ, 686, 279
Koposov S. E., Yoo J., Rix H.-W., Weinberg D. H., Macciò A. V., Escudé J. M., 2009, ApJ, 696, 2179
Koposov S. E., Rix H.-W., Hogg D. W., 2010, ApJ, 712, 260
Koposov S. E., Belokurov V., Torrealba G., Evans N. W., 2015, ApJ, 805, 130
Koposov S. E., Belokurov V., Torrealba G., 2017, MNRAS, 470, 2702
Laevens B. P. M., et al., 2014, ApJ, 786, L3
Laevens B. P. M., et al., 2015, ApJ, 813, 44
Luque E., et al., 2016, MNRAS, 458, 603
Luque E., et al., 2017, MNRAS, 468, 97

Luque E., et al., 2018, MNRAS, 478, 2006
Mackey A. D., Gilmore G. F., 2004, MNRAS, 355, 504
Mackey A. D., et al., 2010, ApJ, 717, L11
Mackey D., Koposov S., Da Costa G., Belokurov V., Erkal D., Kuzma P., 2018, ApJ, 858, L21
Marín-Franch A., et al., 2009, ApJ, 694, 1498
Martin N. F., de Jong J. T. A., Rix H.-W., 2008, ApJ, 684, 1075
Martin N. F., et al., 2016, ApJ, 830, L10
McConnachie A. W., 2012, AJ, 144, 4
Muñoz R. R., Geha M., Côté P., Vargas L. C., Santana F. A., Stetson P., Simon J. D., Djorgovski S. G., 2012, ApJ, 753, L15
Nidever D. L., et al., 2017, AJ, 154
Nidever D. L., et al., 2018, AJ, 156, 131
Ortolani S., Bica E., Barbuy B., 2013, MNRAS, 433, 1966
Otero S. A., 2006, Open European Journal on Variable Stars, 54, 1
Palma T., Clariá J. J., Geisler D., Gramajo L. V., Ahumada A. V., 2015, MNRAS, 450, 2122
Peñarrubia J., Pontzen A., Walker M. G., Koposov S. E., 2012, ApJ, 759, L42
Schlafly E. F., Finkbeiner D. P., 2011, ApJ, 737, 103
Schlafly E. F., et al., 2018, ApJS, 234, 39
Schlegel D. J., Finkbeiner D. P., Davis M., 1998, ApJ, 500, 525
Schmeja S., Kharchenko N. V., Piskunov A. E., Röser S., Schilbach E., Froebrich D., Scholz R. D., 2014, A&A, 568
Shanks T., et al., 2015, MNRAS, 451, 4238
Sitek M., et al., 2017, Acta Astron., 67, 363
Tollerud E. J., Bullock J. S., Strigari L. E., Willman B., 2008, ApJ, 688, 277
Torrealba G., Koposov S. E., Belokurov V., Irwin M., 2016a, MNRAS, 459, 2370
Torrealba G., et al., 2016b, MNRAS, 463, 712
Torrealba G., et al., 2018, MNRAS, 475, 5085
Weisz D. R., et al., 2016, ApJ, 822, 32
Werchan F., Zaritsky D., 2011, AJ, 142, 48
Willman B., 2010, Advances in Astronomy, 2010, 21
Zinn R., 1993, in Smith G. H., Brodie J. P., eds, Astronomical Society of the Pacific Conference Series Vol. 48, The Globular Cluster-Galaxy Connection. p. 38
de Boer T. J. L., Belokurov V., Koposov S., 2015, MNRAS, 451, 3489

APPENDIX A: STELLAR SAMPLE SELECTION

Here we present the catalog-level selections applied to the different surveys to produce clean stellar samples that were then used in the satellite search algorithm.

For **Gaia**, we applied a cut on G between 7 and 21 magnitudes, and selected stars by following Koposov et al. (2017), namely picked objects with $\log_{10}(\text{astrometric\_excess\_noise}) < 0.15(G - 15) + 0.25$. We also corrected for extinction using Schlegel et al. (1998) maps and the Belokurov et al. (2017) extinction coefficient. For **PanSTARRS**, star/galaxy separation was achieved by selected objects with the difference between PSF and KRON magnitudes smaller than 0.05 mags (see Chambers et al. 2016, for details). Additionally, only objects with g and r magnitudes between 14 and 23.2 mags were selected. We also corrected for extinction using the Schlegel et al. (1998) maps and Schlafly & Finkbeiner (2011) coefficients. For **DES**, we used the star-galaxy separation cut suggested by Koposov et al. (2015), and selected objects with magnitudes between 16 and 23.5 magnitudes in g and r filters. Extinction correction was done as above, using an appropriate Schlafly &

Finkbeiner (2011) coefficient for the DES filter set. Finally, for the data from the Mackey et al. (2018) survey, we picked stars with magnitudes between 16 and 23, and used the same star/galaxy separation and extinction correction methods as applied to the DES data.

APPENDIX B: DISCOVERY PLOTS FOR 8 STAR CLUSTERS

The full list of plots summarizing the discovery of the presented objects is given in this appendix.

This paper has been typeset from a TeX/LaTeX file prepared by the author.
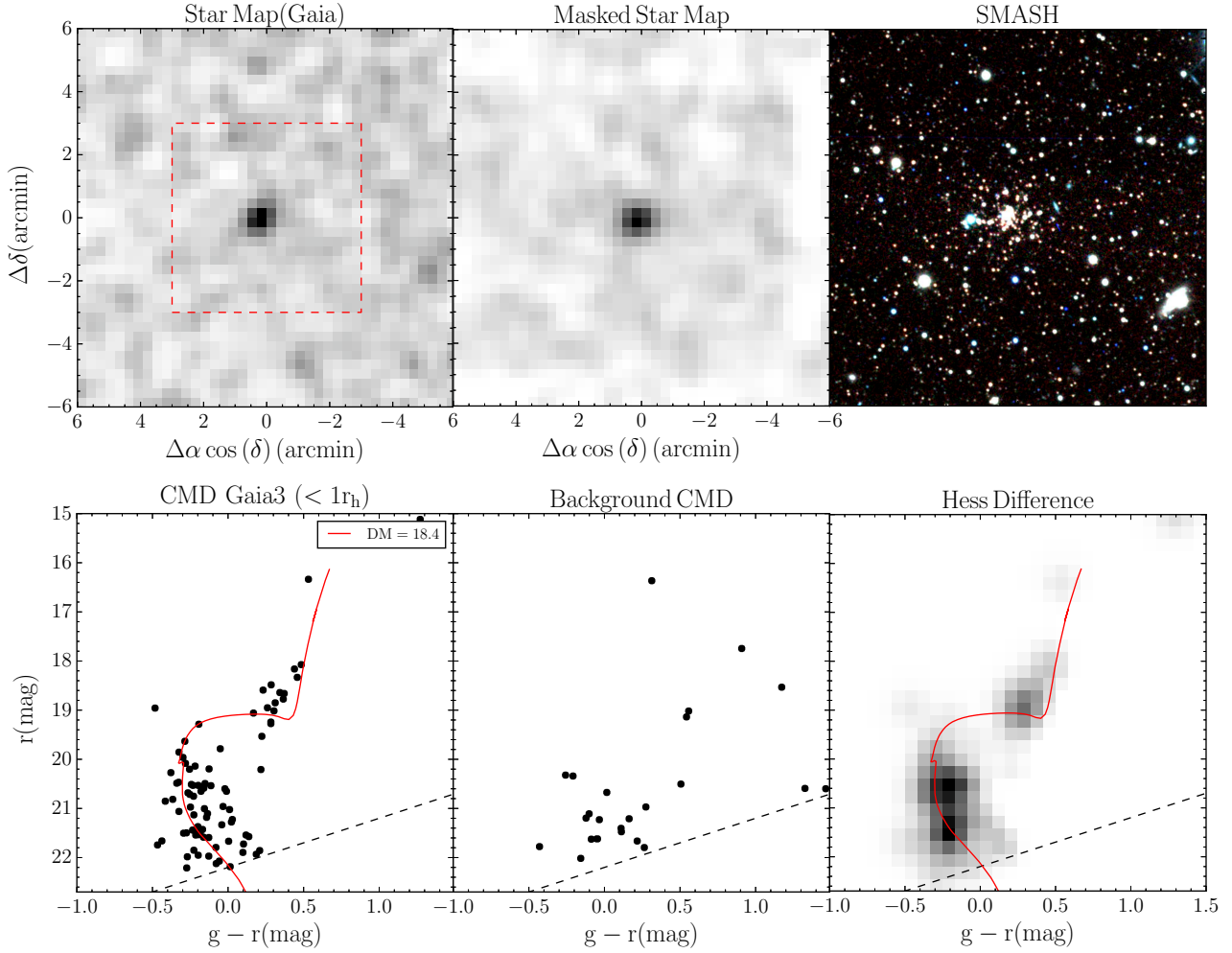
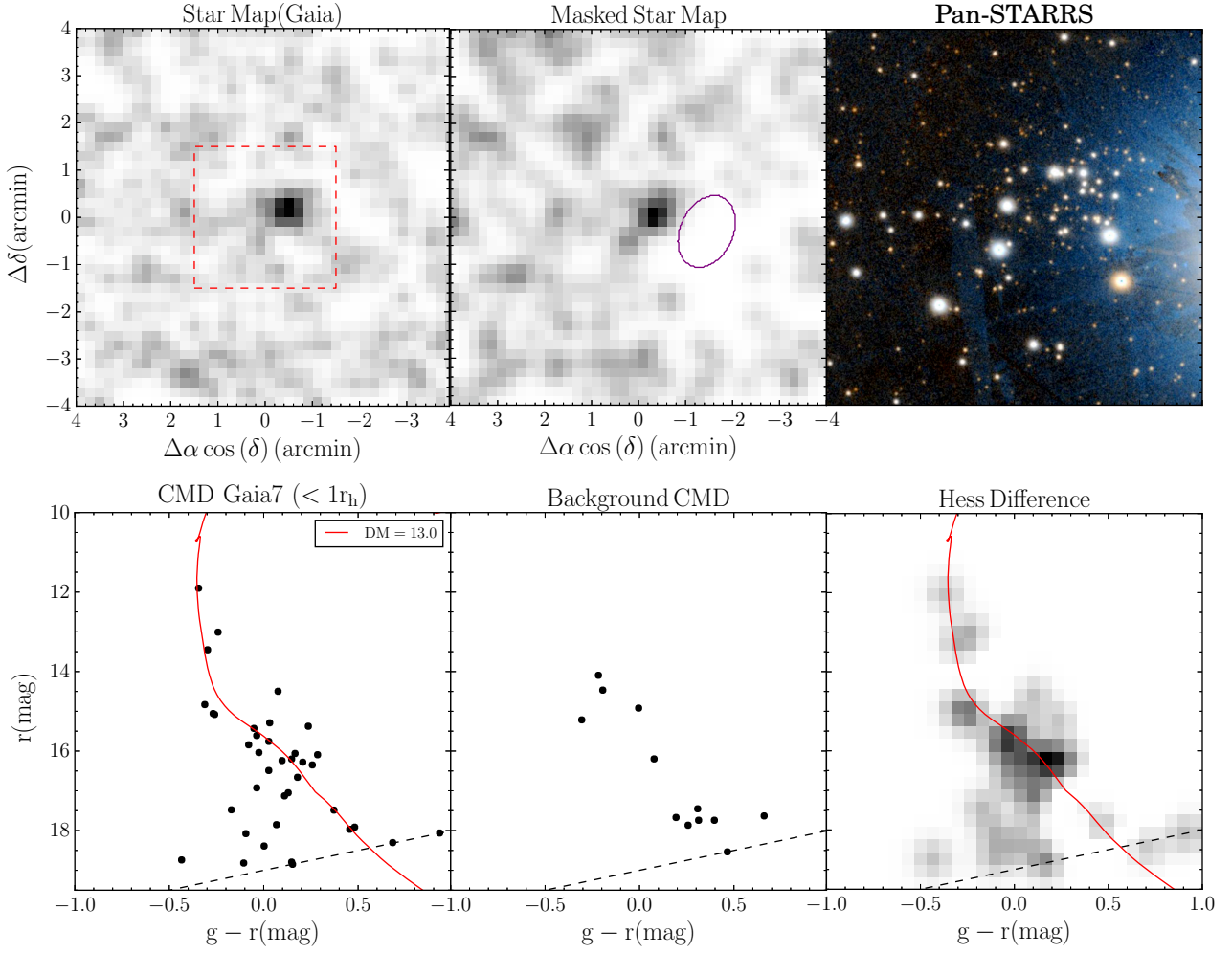**Figure B1.** Discovery plot for Gaia 3. The panels are as described in Figure 3, but with the false color image computed from the SMASH survey. Gaia 3 is only 5.8 deg from the LMC, and at a similar distance ($D_h \sim 48$ kpc) so it is likely a GC that avoided detection due to the high concentration of stars in its center. Nevertheless, by re-analyzing the images from the SMASH survey, we were able to fit an stellar population to the object which is metal poor ([Fe/H] ~ -1.8) with an age of log age~ 9.1 with a total luminosity of $M_V \sim -3.3$ and a size of $r_h \sim 7.5$pc. Its properties, plus the tight concentration of stars at its center, makes Gaia 3 likely a GC associated with the LMC.
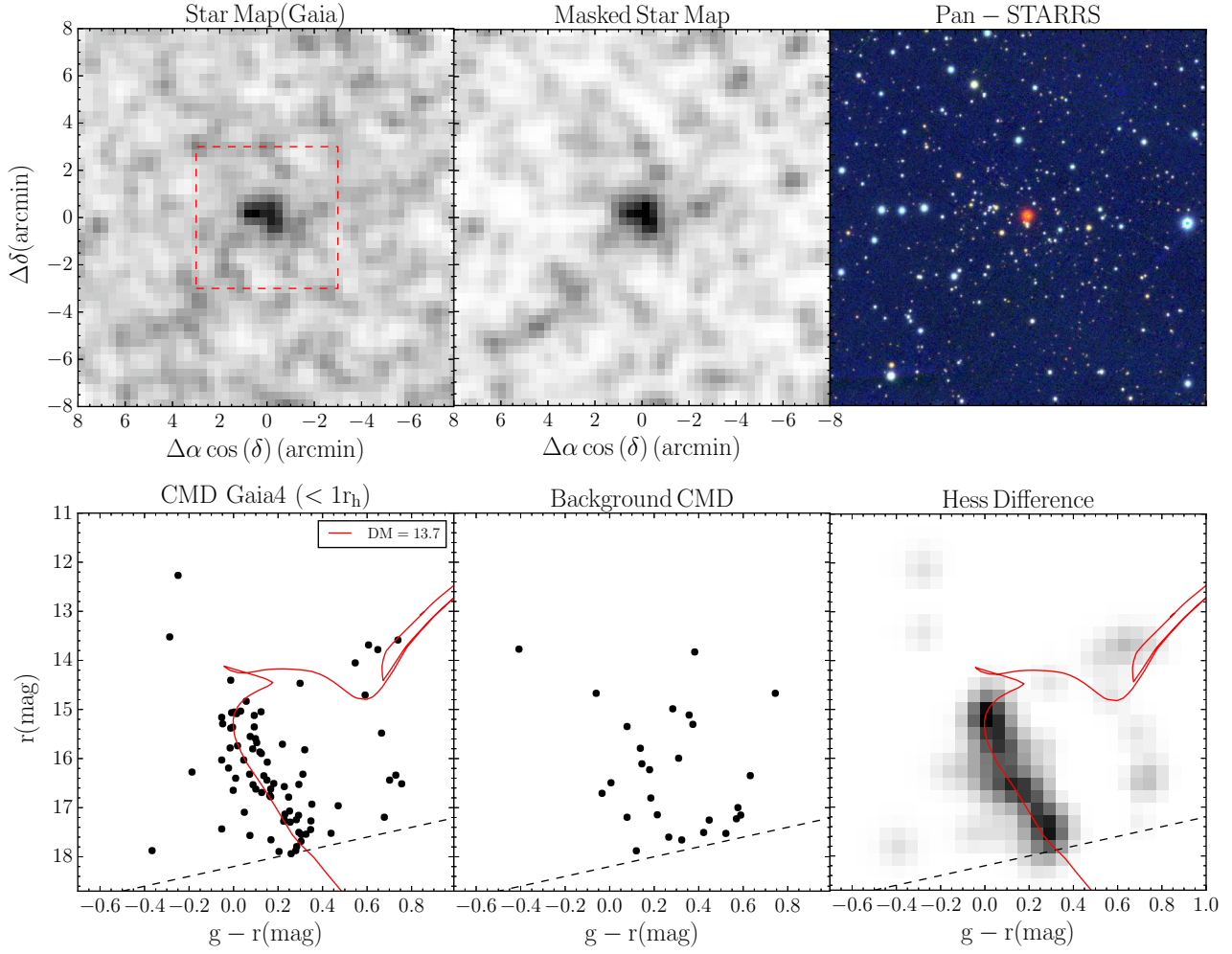
Figure B2. Discovery plot for Gaia 7. The panels are as described in Figure 3, but with the false color image from the Pan-STARRS image server. Gaia 7 is a cluster that hides behind a bright star. In this case, the cluster is within the Pan-STARRS footprint, making it possible to fit an stellar population model to its CMD, which is fully consistent with an OC classification. The purple circle in the middle top panel marks the region around the bright star that we masked out when doing the fitting.

Figure B3. Discovery plot for Gaia 4. The panels are as described in Figure 3, but with the false color image from the Pan-STARRS image server. Gaia 4 is also within the Pan-STARRS footprint, sitting in the Galactic disk ($b \sim -1.5$) at a region of very high extinction. The overdensity of stars is very prominent both in Gaia and Pan-STARRS, with a very well defined MS, making it the brightest of the objects presented in this paper with $M_V \sim -2.4$.
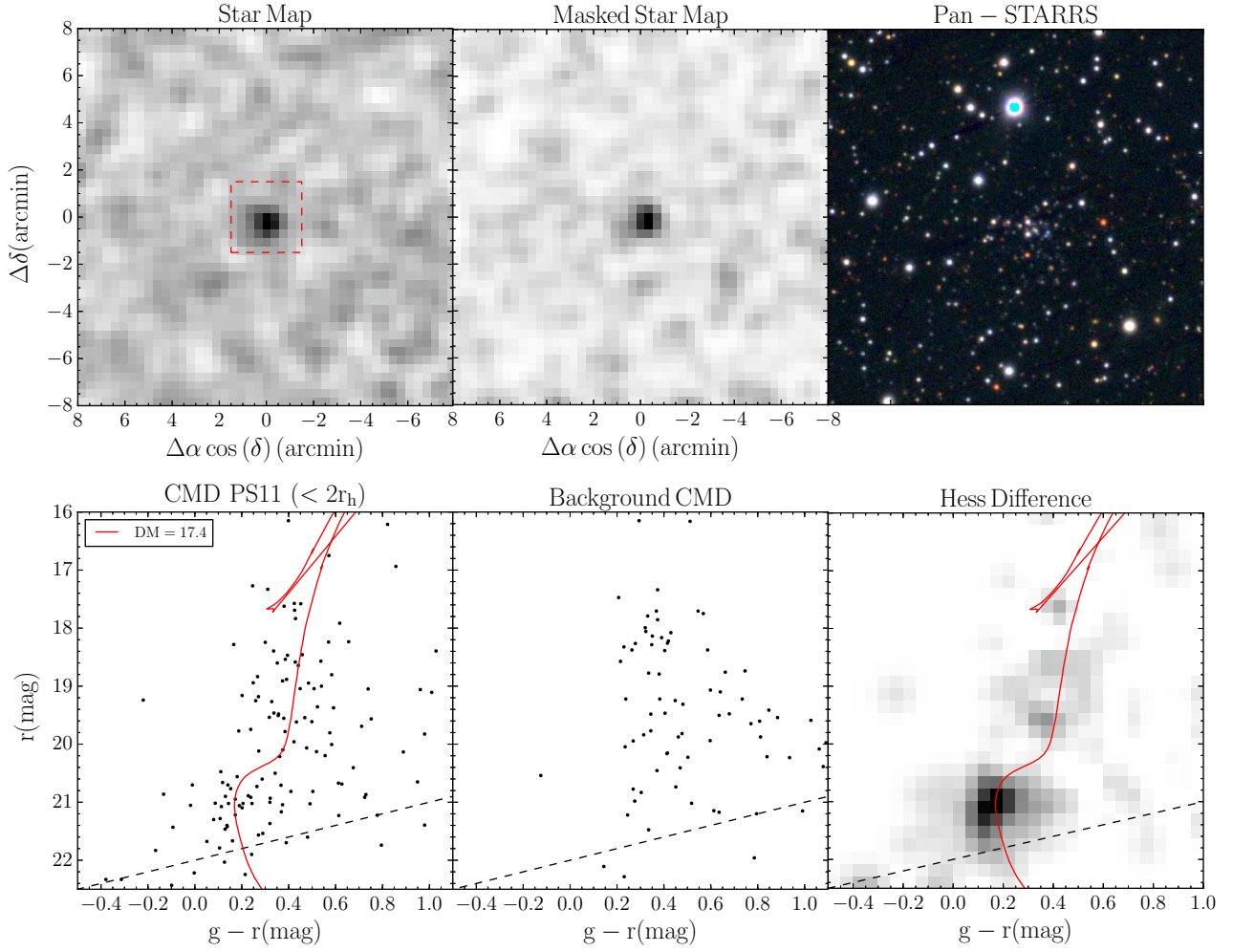
Figure B4. Discovery plot of PS1 1. The panels shows Pan-STARRS data release 1 observations, and are as described in Figure 3. In this case, the Masked star map is only showing MSTO stars. PS1 1 spatial overdensity is evident both in the images and in the density maps. A conspicuous accumulation of stars in the CMD at the position of the MSTO, where no much background stars are expected, can also be seen.
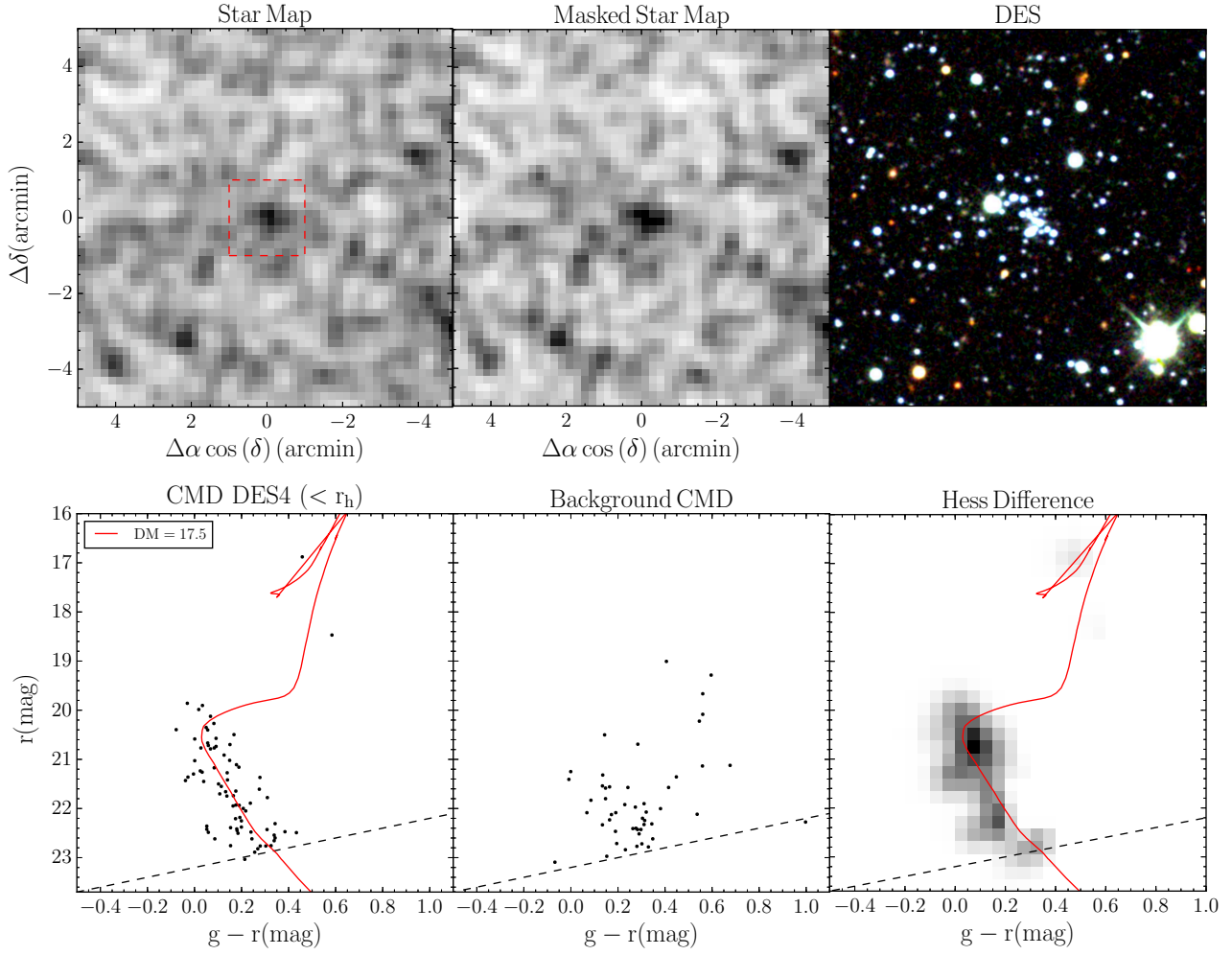
Figure B5. Discovery plot of DES 4. The panels shows Koposov et al. (2015) version of DES, and are as described in Figure 3. Event though the density map marginally shows an overdensity, the false color image highlights a conspicuous overdensity of stars. The contrast is likely due to missing stars because of crowding. DES 4 is located next to the LMC. This can be seen in the CMDs of the object and the background. Even so, an extended MSTO reveals DES 4 in the CMDs as formed by a young population, like many of the LMC clusters.
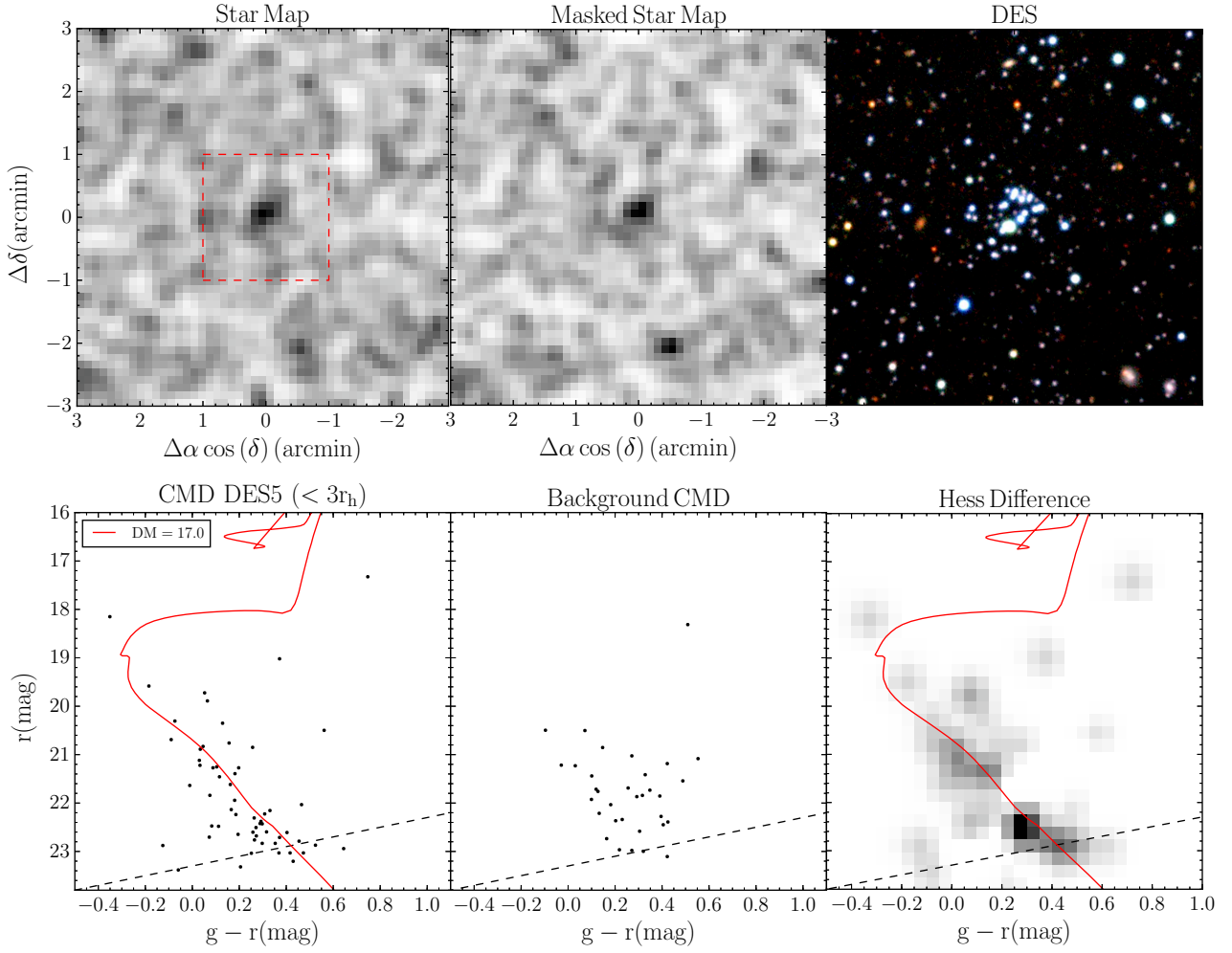
Figure B6. Discovery plot of DES 5 as seen with DES DR1 data. All panels are described as in Figure 3. The false color image alone can confirm Des 5 as a distinct group of stars, but it is also seen as a conspicuous overdensity of stars in the density maps. The extended main sequence, compared to the background, allows to constrain the distance to Des 5 at 25 kpc. Located only ∼ 7 deg away from the LMC, the position of DES 5 is consistent with being part of the LMC GC population.
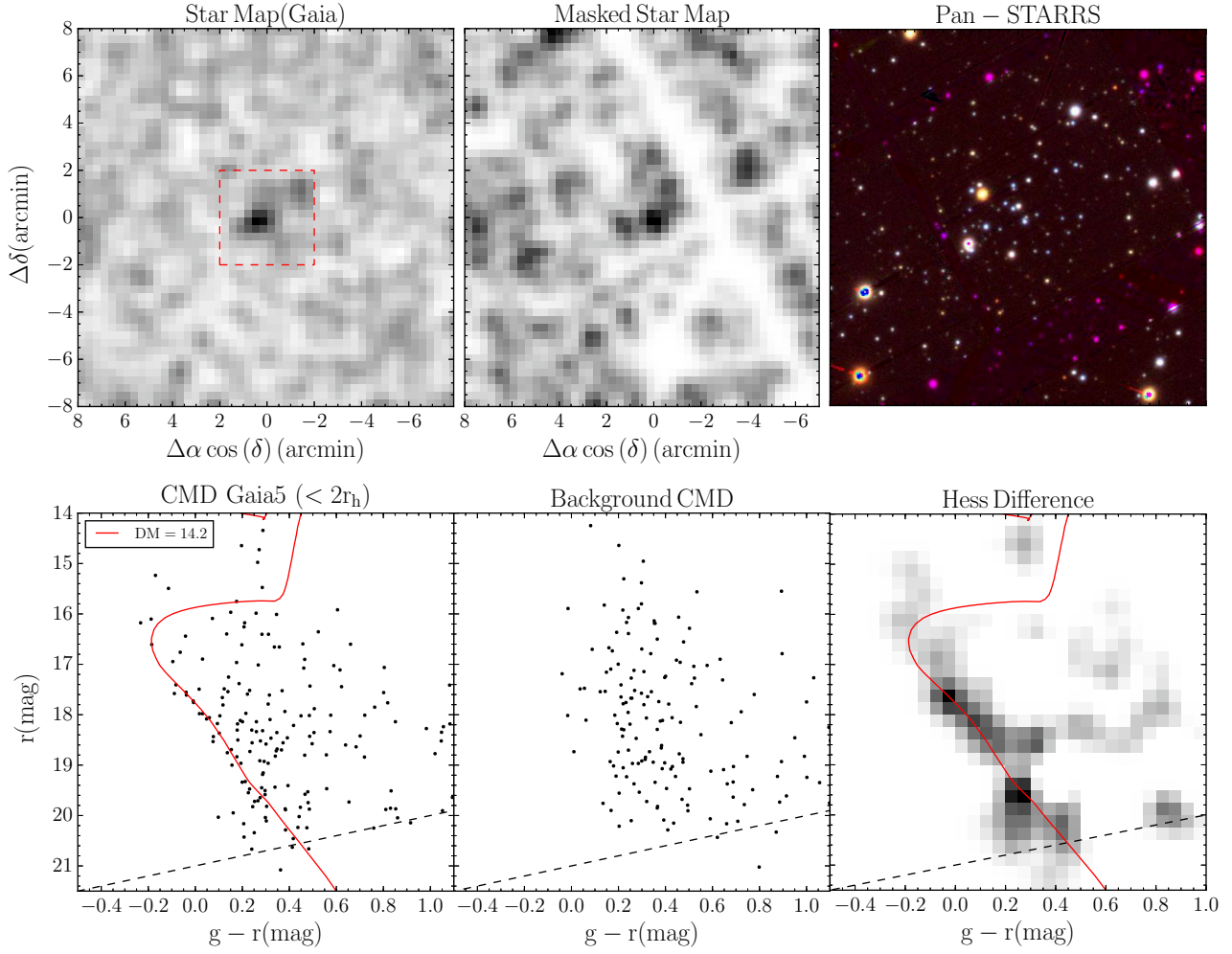
Figure B7. Discovery plot of Gaia 5. Top left panel shows a density map of Gaia stars, while the rest of the panels shows Pan-STARRS data. All panels are described as in Figure 3. Gaia 5 reveals itself unambiguously in the Gaia density map of stars, but due to incomplete data and high extinction in the region, it was not originally found in Pan-STARRS. The hints of a distinct group of stars in the false color image, as well as the young main sequence seen in the CMDs suggests that Gaia 5 is likely a genuine satellite. Gaia 5 is located very close to the Galactic disk at $b \sim -7 \deg$, added to its properties, it looks like it belongs to the Galactic disk open cluster population.
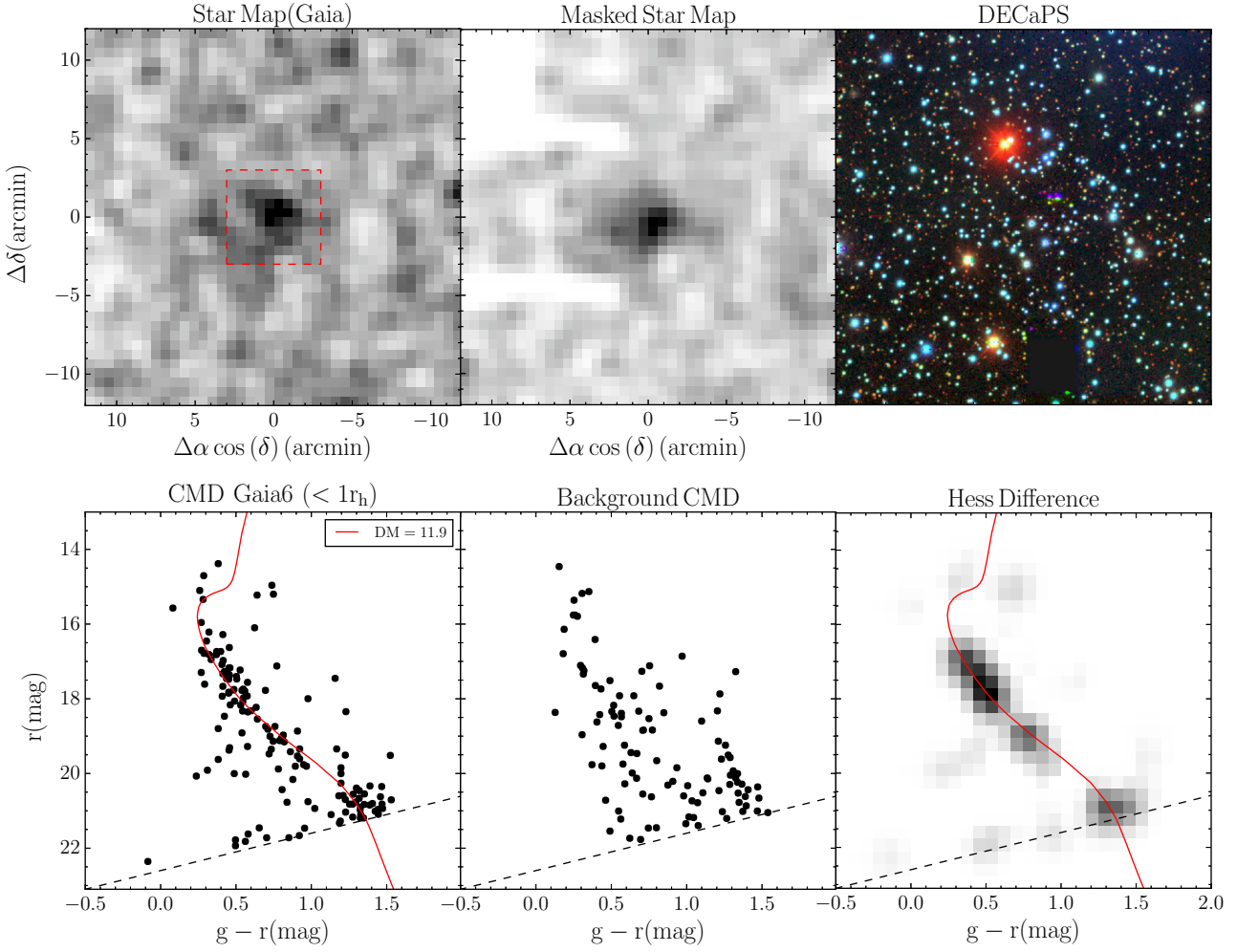
Figure B8. Discovery plot of Gaia 6. Top left panel shows a density map of Gaia stars, while the rest of the panels shows DECaPS data. All panels are described as in Figure 3. Like Gaia 5, Gaia 6 is also within the Pan-STARRS footprint, but we only found the overndeisty in Gaia data. Noticeable features in the CMD, a clear overdensity of stars in both datasets, and hints of a distinct group of stars in the false color image, points out to Gaia 6 as a real stellar system. Gaia 6 is also close to the Galactic disk with properties that are consistent with an open Galactic cluster.